LESSONS LEARNED FROM OPERATING THREE CUBESATS UNTIL THEIR CONSECUTIVE RE-ENTRIES

Julian Harbeck[†], Anton Johann Große Siestrup[†], Victoria Koßack[†], Oisín Smith[†], Linus Streibert[†], Tony Erdmann [†], Sascha Kapitola[†], Sebastian Grau[†], Enrico Stoll[†]

[†]*Technische Universität Berlin, Chair of Space Technology, Marchstr. 12-14, D-10587 Berlin, +49 314-21623, harbeck@tu-berlin.de*

April 15, 2024

Technische Universität Berlin's mostly COTS based 1U CubeSat series "BEESAT", was launched over the last decade. After outliving their primary mission, operations were taken over by the student operations team StudOps and in the scope of lectures. Three of these missions recently came to an end-of-life through natural decay within a six-month period. This provided the opportunity to observe the satellites behavior prior to and during early re-entry. Furthermore, lessons learned during previous re-entries could be imminently applied to subsequent re-entries. The state of the BEESAT satellite bus is assessed after operating for a decade in orbit and the remaining orbit dwell time is continually predicted. Increasing spin up is observed in the days leading up to the re-entries. The SatNOGS network of amateur radio ground stations is involved to track the satellites. It can be confirmed that the tracking of the satellites as well as Doppler shift corrections are a challenge during the final days in orbit as TLEs provided by NORAD outdate rapidly. Further measures to track the satellites directly via radio frequency satellite tracking are evaluated. Lessons learned from the re-entries of BEESAT-2, -3 and -4 will be applied to upcoming re-entries like the one of BEESAT-9.

1 INTRODUCTION

This work documents lessons learned from operating three CubeSats of the Berlin Experimental and Educational Satellite (BEESAT) series of Technische Universität Berlin (TU Berlin) until their consecutive re-entries in the span of a few months around the turn of the years 2023/2024. This introductory section presents the operated satellites and the bus they share, motivates the operation until their re-entries and gives an overview of the structure of the paper.

1.1 The BEESAT Satellites

With the development and launch of their first 1U CubeSat BEESAT in 2009, TU Berlin adapted early to this novel standard after pioneering in the development of small satellites in the academic domain with the launch of the first TU Berlin Satellite (TUBSAT) in 1991. Developed as technology demonstration missions, the 1U BEESAT series laid a foundation in the miniaturization of satellite technologies which enabled missions such as Nanosatellites in Formation Flight (NanoFF) [1], recently launched as the 28th and 29th TU Berlin satellites. The mostly redundantly designed BEESAT satellite bus turned out to be reliable and extendable as four iterations of the bus were developed and

launched in the following years. The BEESATs operated in orbit successfully and beyond their usual planned operational phase of one year.

The successors BEESAT-2 and -3 were launched together on the same rocket in 2013. BEESAT-2 was building directly on the first BEESAT not only demonstrating the reaction wheels specifically developed for this purpose like the predecessor, but demonstrating full three axis attitude control as well as introducing a dedicated payload board with an optical camera to the bus [2].

BEESAT-3 differs form other BEESATs as it was developed mainly by students in the scope of an educational project. The bus is simplified by removing the redundancies of many subsystems and changing to a passive attitude control. On the other hand it features a S-Band-downlink transmitter as payload. BEESAT-3 was long considered a failure until the first contact was finally realised after more than five years in orbit in 2018 [3].

The direct successor of BEESAT-2 was BEESAT-4, launched inside the Deutsches Zentrum für Luft- und Raumfahrt (DLR) satellite Bi-spectral InfraRed Optical System (BIROS) as a passive counterpart for formation flight maneuvers [4]. It features capabilities to establish an inter-satellite-link and a Global Positioning System (GPS) receiver as additional payloads [5]. All of these introduced BEESATs were operated until their recent re-entries. An overview is given in Table 1.

Table 1: Overview of the three BEESAT 1U CubeSats and their Subsystems

	BEESAT-2	BEESAT-3	BEESAT-4
Launch date	2013-04-19		2016-07-05
Orbit	inclination: 64.9°, altitude: 515 km		SSO at 500 km
Mass	990.0 g	922.9 g	1030.0 g
Attitude determination	MEMS-gyroscopes, 6 sun sensors	Gyros, sun sensors	MEMS-gyroscopes, 6 sun sensors
Attitude control	3 reaction wheels, 6 magnettorquer	permanent magnet, hysteresis plate	3 reaction wheels, 6 magnettorquer
Communication	glsuhf 435.9485 MHz 2 monopole antennas	glsuhf 435.95 MHz 1 monopole antennas	glsuhf 435.95 MHz 2 monopole antennas
Payload	Camera	Camera, HiSPiCO S band transmitter (2.263 GHz)	Camera, Phoenix GPS receiver
Mission objective	Advanced attitude stabilization	Education of students	Precise positioning and orbit determination
Operated by StudOps	since 2022-12	since 2023-02	since 2022-01
Re-entry	2024-02-01	2023-12-28	2023-09-23

The operations of the satellites until their end-of-life through natural decay and re-entry could be realized due to the robustness of the BEESAT satellite bus and by involving students into operations. Therefore, starting with BEESAT-4 in 2019 these still operational satellites were integrated into student education after they fulfilled their primary missions objectives [6]. These hands-on activities were further developed and more satellites were opened up for students enabling them to gain additional scientific value from these missions [7]. In the recent years, the newly founded TU Berlin Student Satellite Operation Team (StudOps) took over the routine operations of the satellites and conducted the experiments concerning the re-entries documented in this work.

1.2 The Re-Entry - a New Regular Mission Phase in the Satellite Life Cycle

As more and more satellites and constellations are launched into Low Earth Orbit (LEO) with orbit heights above 500 km the risk of collisions and the overall amount of space debris arises. Therefore,

recent research aims to open up the Very Low Earth Orbit (VLEO) for applications [8]. The VLEO has the advantage but at the same time challenge that orbits decay rapidly due to the denser atmosphere. Space Debris therefore re-enters faster and it is easier to comply with regulations. However, to operate space systems here they most likely require a propulsion system and need to withstand the harsher orbit environment [9]. Operating the BEESATs during their decay through this orbit region and conducting specific experiments shall contribute to endeavours to understand VLEO and satellites' re-entry processes better. It also prepares for future missions which will more often be operable in this region when launched to lower orbits in the beginning.

1.3 Overview of this Paper

The first part of the paper in Section 2 tackles the overall challenge to evaluate the remaining operational lifetime by predicting the exact re-entry date for satellites and how it was solved for the BEESAT re-entries. A status update on the different BEESAT spacecraft and their subsystems after years in orbit is given in Section 3. The planning of the End Of Life (EOL) operations is documented in Section 4. Findings and challenges of this ops campaign are discusses in Section 5 concerning the mitigation of two-line element (TLE) inaccuracies and in Section 6 observing a spin-up of the satellites during the final days of operations.

2 PREDICTING SATELLITE RE-ENTRIES

An obvious precondition to being able to plan re-entry operations is being able to estimate when the re-entry will take place. This is a non-trivial problem due to significant uncertainty in several factors like solar activity, aerodynamic properties of the spacecraft, atmospheric density modeling, and others [10]. As time goes on, the remaining time decreases and thus the absolute error in re-entry time tends to decrease [11]. As such, starting with BEESAT-3, an automated system was developed to regularly recompute predictions based on the latest orbit parameters available from North American Aerospace Defense Command (NORAD) and the latest space weather predictions.

At regular intervals, TLE data is queried from Celestrak [12]. If new TLE are available, the computation of a new prediction is initiated. First, the latest space weather data is downloaded. Next, the TLE data is converted to a state vector for use with NASA's General Mission Analysis Tool [13]. A script is generated based on a template using the new state vector, spacecraft mass, aerodynamic parameters, and space weather data. The spacecraft state is then propagated until the altitude of the satellite falls below approximately $180\,\mathrm{km}$ above sea level. It is expected that from this altitude, decay will occur within hours [14] and this point in time is defined as the predicted re-entry time.

Operators are informed of the new simulation results by an automated notification. To avoid overloading operators with useless information, like a one hour change in predicted re-entry time three months ahead of the predicted re-entry time, which has no impact on planning, notifications are filtered. The implied currently remaining lifetime of the spacecraft based both on the last prediction that operators have been notified of and the prediction that was just generated is calculated. If these times differ by a threshold of more than 10% or less than 24 hours remain until the predicted re-entry time, a notification is dispatched and the local copy is updated. Otherwise, the notification is discarded.

Spacecraft-specific ballistic parameters are derived using a manual calibration process. First, the dry mass of the spacecraft is set based on ground measurements before launch. A fixed drag coefficient of 2.2 is assumed. Next, an initial estimate for the average aerodynamic drag area of the spacecraft

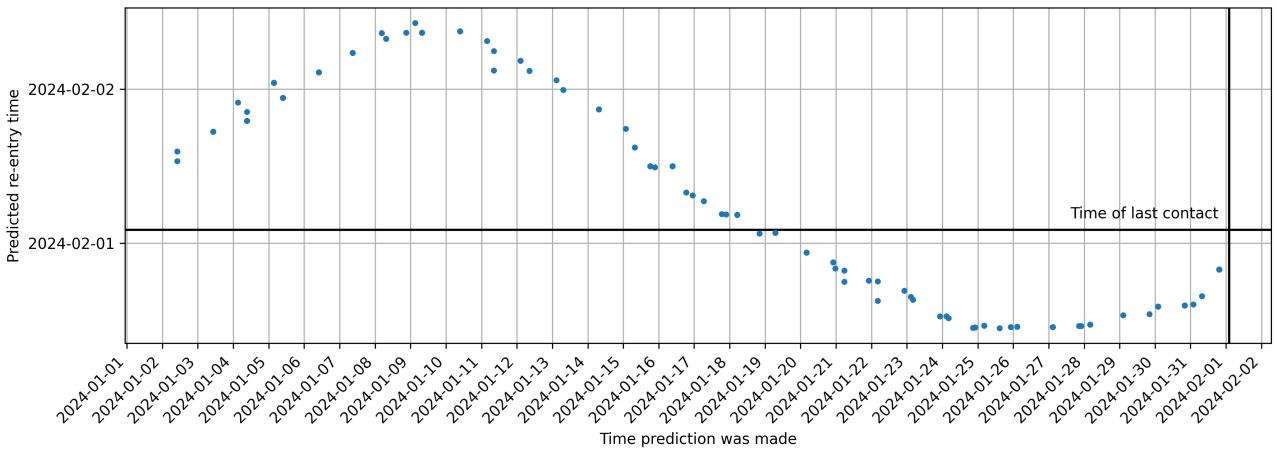

Figure 1: BEESAT-2 Re-Entry Time Predictions over Time

is derived using estimates, e.g. for a cube with side length $10\,\text{cm}$ at a random orientation, an average drag area of $\frac{1}{4} \cdot 6 \cdot (10\,\text{cm})^2 = 0.015\text{m}^2$ can be estimated using Cauchy's surface area formula [15]. Next, instances of the simulations are initiated n times using historical orbital parameter data of the spacecraft state from times $t_i = t_{now} - T_{bias} - i \cdot T_{offset}$, with $i \in \{1, \ldots, n\}$, t_{now} being the current time, T_{bias} and T_{offset} being chosen parameters. The simulations are ran until time $t_{stop} = t_{now} - T_{bias}$. This excludes a part of the available data from the calibration process. The excluded data can later be used to verify the accuracy of the model without being affected by potential overfitting. The same set of historically known space weather data is used for all simulations to remove this uncertainty from the calibration process. The simulation results are compared with each other. If an overall downwards trend is visible in the results, i.e. as i increases, the predicted semi-major axis at time t_{stop} tends to decrease, then the used drag area value is increased. And vice versa if as i increases, the predicted semi-major axis at time t_{stop} increases, then the used drag area value is decreased. The simulations are then repeated using the adjusted drag area value, and the process is repeated until it converges. The quality of the solution can then be assessed by comparing the predicted semi-major axes at time t_{stop} with the known historical value. If an unreasonable error is present, the calibration can be rejected. Additionally, the simulations can then be propagated forward to time t_{now} using the chosen set of parameters and checked against the current orbital parameters. If an unreasonable error is present here, the results can again be rejected. This reassures the soundness of the calibration process and detects an overfitting of the parameters. Nevertheless, this manual process presents a significant source of error and automating this process should be considered in future.

As an example result the predicted re-entry date over time for BEESAT-2 can be seen in Figure 1. There is a variation of approximately two days in the results, however overall, the predictions proved fairly accurate, as the last reception of BEESAT-2's signal occurred on 2024-02-01.

3 STATUS of the BEESAT-BUS AFTER YEARS in ORBIT

Shortly prior to the re-entry the status of the BEESATs is assessed. The performance of the attitude determination and control system (ADCS) and its reaction wheels is evaluated. Electrical Power System (EPS) telemetry of one satellite's lifetime is analysed for signs of degradation.

3.1 Attitude Determination and Control Subsystem

For three axis attitude control BEESAT-2 and -4 feature three reaction wheels, one mounted along each body axis. These wheels were used throughout the entire mission duration.

With BEESAT-4 a differential drag campaign stress tested the ADCS onboard with a nadir pointing maneuver during every orbit. In total performing around 1000 nadir pointing maneuvers in the months leading up to re-entry. During this campaign no deterioration of the ADCS was observed. The analysis of the differential drag campaign will be the focus of a different publication.

To evaluate the performance of the reaction wheels after almost 11 years in orbit, the wheels onboard BEESAT-2 are commanded to run a along a predetermined test trajectory. This test trajectory is run once with each wheel individually and once with all wheels simultaneously. During the entire experiment the rotational speed of the wheels and the angular rate of the spacecraft is recorded at 1 Hz. The same test trajectory was also run with all wheels simultaneously in December 2019, providing a baseline for evaluating possible degradation in the 4 years since. The result of these tests can be seen in Figure 2. No degradation is visible between the test in 2019 and the test shortly before re-entry in 2024. Additionally a spin of the spacecraft around the respective axis in the opposite direction is clearly visible in the single wheel tests performed during the 2024 test. Additionally it is visible that the maximum angular rate reached by the spacecraft is lowest on the Z-axis, where the inertia of BEESAT-2 is highest (see Equation (3)).

The initial commissioning of the reaction wheels onboard BEESAT-2 was done by directly commanding rates to individual wheels without using the integrated predetermined test trajectory. As this is difficult to accurately reproduce, the tests performed as part of the EOL campaign can not be directly compared to the tests performed during commissioning.

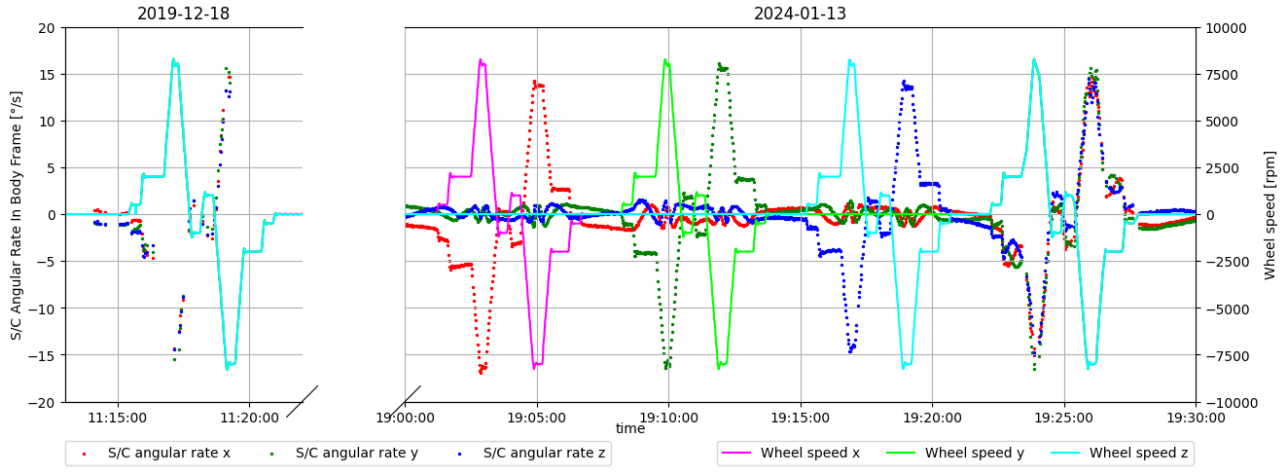

Figure 2: Tests Performed with the Reaction Wheels Onboard BEESAT-2

3.2 Electric Power Subsystem

The mission design lifetime of the BEESAT satellites was one year and the electronics design makes use of Commercial-off-the-shelf (COTS) components as much as possible. Therefore, an analysis of some subsystems' currents is done to understand the long-term behavior of the components especially under the harsh conditions in space. Figure 3 shows the currents of the Power Control Unit (PCU), Transceiver (TRX), and Payload Data Handling (PDH) subsystems over the whole orbital lifetime of BEESAT-4. It is generated by using daily averages of the currents from all available data packets of the mission. The shown values are all in the expected range and it can be seen that no big deviation was observed over the lifetime of the CubeSat. The current of the PCU is mainly stable at around 14 mA but shows some small variations. These are reasoned by different loads of the microcontroller unit (MCU) during the sampling of the current. The visible gaps in the data are mainly explained by the fact that the satellite was not operated during that time. Especially, the PDH current clearly depicts time frames of

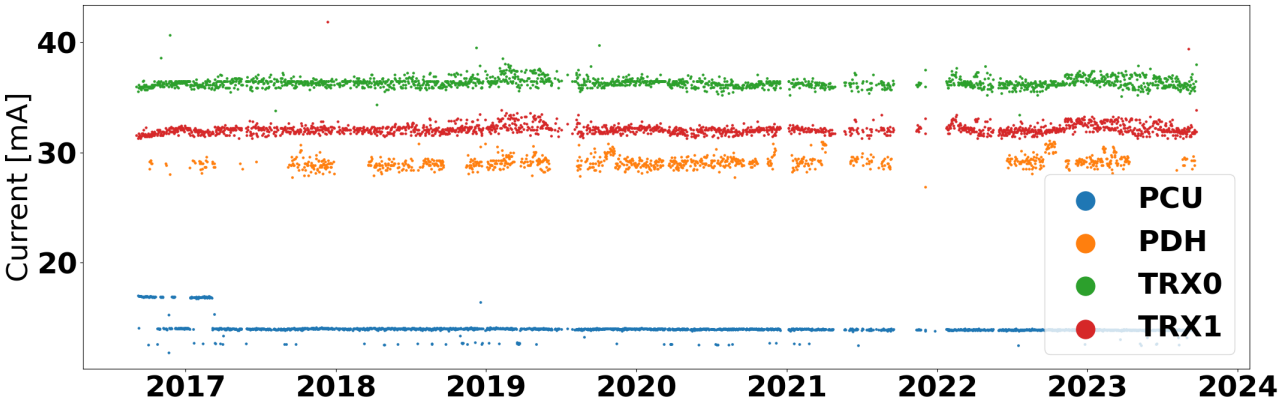

Figure 3: Currents of BEESAT-4 Subsystems

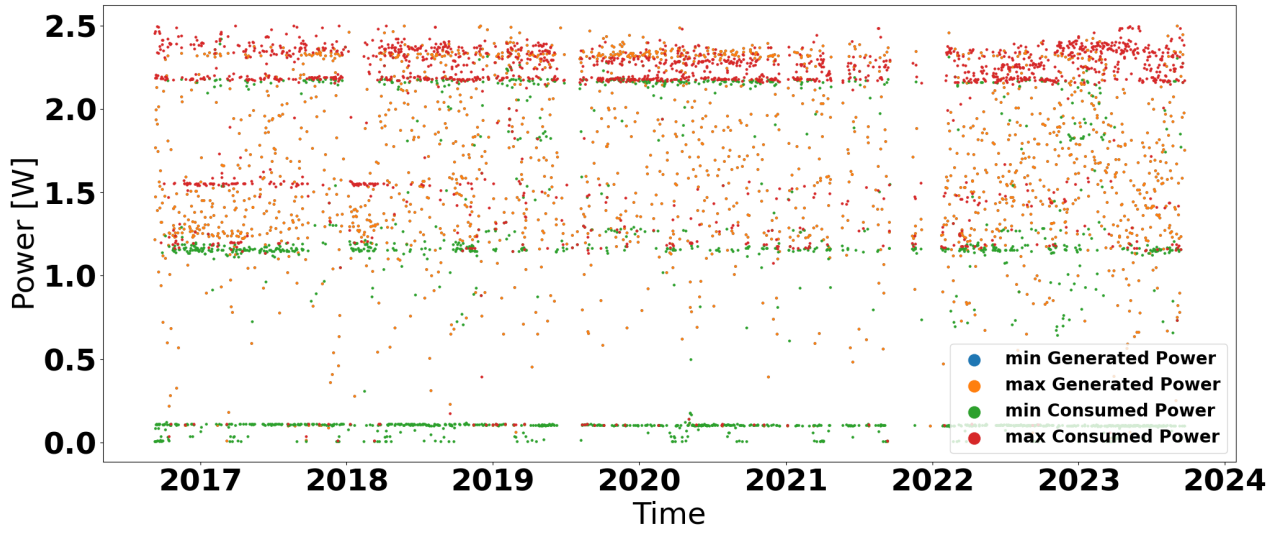

Figure 4: Power Generation and Consumption of the BEESAT-4 Satellite

reduced operation activities, e.g. in mid 2019, when BEESAT-9 was launched and the operations team focused on the Launch and Early Orbit Phase (LEOP) of that mission.

Figure 4 gives an overview of the amount of generated and consumed solar power of BEESAT-4. Daily values of the minimum and maximum generated and consumed power are shown. Consumed solar power refers to the power that is immediately transferred from the solar cells to the batteries and/or the system. The plot shows a maximum power generation value of around 2.4 W which represents an expected value of the implemented solar cell configuration. Over the orbital lifetime of around seven years, no degradation of the solar power generation is observed. The maximum generated power is the same at the beginning and at the end of the mission. The figure shows an accumulation of values for the minimum consumed power at around 1.15 W. This corresponds to the power required to charge one of the two batteries. The values $\leq$100 mW show times when the batteries are not charged at all or the satellite is in eclipse. In summary, the power generation of all BEESATs proofed to be stable throughout the orbital lifetime of the satellites. The power budget was positive through all operational phases. Phases of higher loads and with a slightly negative power budget (e.g. long pointing maneuvers) could easily be compensated by the batteries and re-charge times in subsequent Sun phases.

4 END OF LIFE OPERATIONS

Monitoring the remaining orbital lifetime of TU Berlin satellites was a work package regularly conducted by students within the project lab Satellite Operations (SatOps) lecture [16]. It was therefore longer known that BEESAT-4 will be the first BEESAT satellite to re-enter into Earth's atmosphere in 2023. Although the predictions are subject to inaccuracies as described in section 2, crossing an altitude of 400 km in May 2023 was used as a starting point to perform regular analyses and plan the end of life operations.

As seen in Section 3 the BEESAT satellites were functional for multiple times longer than their design lifetime and where in active operation. With the forecasted re-entry date approaching, the StudOps team responsible for the operations defined two main objectives for the re-entry campaigns:

- Study the re-entry phase as a unique operational phase
- Acquire scientific data until the last possible moment before re-entry

This subsection documents the process and results of the EOL operations.

4.1 Utilizing the Open Ground Station Network SatNOGS

Satellite Networked Open Ground Station (SatNOGS) is a open ground station network allowing amateur radio operators around the world to participate and contribute to the observation of satellites transmissions [17]. In its simplest design a ground station consist of an omnidirectional antenna, a software-defined radio (SDR) and a small single-board computer, for example a Raspberry Pi, making the setup of one very affordable and the entry barriers low. The observation of a satellite from one or more ground stations, that support the satellites frequency band, can be scheduled easily through a web interface or an application programming interface (API). An observation is a Doppler shift corrected recording of spectral data at a specified frequency and bandwidth. Therefore, one can easily see if a satellite is transmitting data by looking at the waterfall diagram of the recorded data. In the context of re-entry operations this is helpful to detect if a satellite is transmitting at all, as communication problems can also have other reasons as discussed in Sections 4.4 and 5. It is also possible to decode the telemetry directly since the communication protocol and telemetry format must be published if amateur radio frequency bands are used, according to International Telecommunication Union (ITU) Radio Regulations [18].

Challenges in the utilisation of SatNOGS in the context of re-entry operations arise from the implementation of scheduling observations. SatNOGS ground stations perform observations based on a pre-calculated time span that they are given during scheduling, not the current TLE of a satellite. Changes in the satellites orbit after the time span was calculated are not considered. As discussed later in Section 5,changes in the orbit happen rapidly during the EOL. Since recalculation can only be triggered by a SatNOGS administrator, it is advised to either schedule only shortly before an observation or to get in touch with them early on. Additionally it can be challenging to deploy telemetry decoders to a large number of ground stations as the software running on them is fragmented over many versions.

To receive signals via the SatNOGS ground station network automatic transmission of telemetry is activated onboard the BEESATs in the days before re-entry. Automatic telemetry transmissions are only commanded to take place while the spacecraft is over SatNOGS stations. This is done to prevent unnecessary interference with other signals in the frequency band as well as to preserve power onboard the spacecraft. Overall SatNOGS provided a very valuable service to all BEESAT re-entry campaigns.

4.2 Record and Decode IQ Data

As results from a SatNOGS observation, audio data centered on the transmit frequency of the spacecraft after Doppler correction using the available TLEs is available. Additionally, in-phase and quadrature components of a radio signal (IQ) data was made available from select stations by their respective operators. Some stations may also attempt to directly decode telemetry using an existing open source decoder based on GNU Radio [19]. However in the case of the BEESAT family, only a minority of ground stations currently implement this capability. Consequently, manually running the decoder is required in most cases.

However, with the quickly aging TLEs (see Section 5), the accuracy of the Doppler correction in these recordings is low. As a result, frequency errors as high as approximately 10 kHz [20] occur, which the existing decoder could not support. To address this, a new pipeline was set up that would automatically detect energy bursts in the radio frequency (RF) spectrum corresponding to transmitted telemetry frames, estimate the frequency and correct it to baseband. From there, the telemetry was FM-demodulated and decoded. This allowed extracting telemetry data from several recordings with significant frequency error due to Doppler shift.

4.3 Making Necessary Compromises

On the BEESATs telemetry in stored in a First In First Out (FIFO) memory. So in order to download the scientifically more interesting telemetry shortly before the re-entry, the onboard telemetry buffer is emptied in preparation of the EOL operations. From this point it is attempted to not generate more telemetry than the downlink budget allows to be downloaded. To achieve this, some telemetry had to be deleted onboard BEESAT-2 to -4.

The Communication System (COM) of BEESAT-2 and -4 feature a protocol (*COM acknowledge*) where the ground station acknowledges every received telemetry frame with a short message to the spacecraft. This system prevents the deletion of telemetry onboard the satellite that was not received by the ground station. If the satellite does not receive the acknowledgment from the ground station, already received telemetry from the onboard buffer is transmitted again. The overhead of transmitting some frames multiple times is acceptable during nominal operations, where it is more important to receive the complete telemetry, rather then risk deleting important telemetry.

In order to receive as much unique telemetry frames as possible, the *COM acknowledge* protocol was disabled at several points throughout the last 48 h of operations. During the EOL operations, the result of the trade off between data integrity and data throughput is different, as the spacecrafts remaining orbital lifetime is limited. Therefore it is more important to receive unique data in every frame to have as much telemetry from the time in VLEO as possible. With SatNOGS ground stations simultaneously recording data, it is possible to retrieve some frames not received by the TU Berlin ground stations.

4.4 Operating BEESAT-3's S Band Transmitter

As mentioned in Section 1.1 BEESAT-3 features a high-speed S band transmitter. It allows the downlink of payload data with higher data rates as the ultra high frequency (UHF) telemetry link. For the first time since the commissioning of the spacecraft in 2018 [3], the Hochintegrierter S-Bandsender für Pico- und Nanosatelliten (HiSPiCO) S band transmitter was activated in spring 2023 in preparation of BEESAT-3's 10^{th} orbit anniversary. It was shown then that the transmitter is still capable of transmitting images taken by the spacecraft even after a decade in space. In preparation of the re-entry campaign it was attempted to operate the S band transmitter as long as possible, while also trying to analyse the link quality.

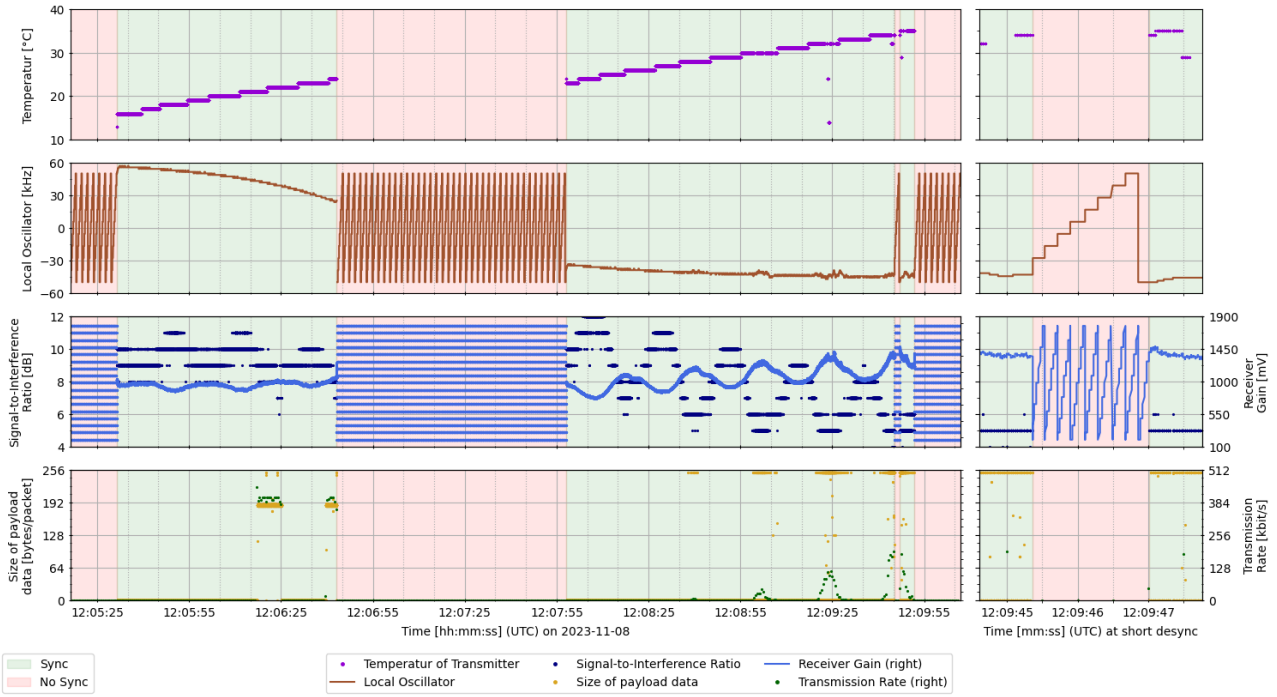

Figure 5: Status Data of the HiSPiCO S Band Transmitter and Receiver During a Pass on 2023-11-08. On the Right Side an Excerpt from the Graph Shows a Short Desync with Higher Temporal Resolution.

Figure 5 shows the status data from the HiSPiCO receiver from a pass conducted on 2023-11-08. The times with sync to the spacecraft's transmitter are shaded in green while the times without are in red. It should to be noted that the S band transmitter on BEESAT-3 is turned off automatically after 2 min to prevent permanent activation which would cause a problem for the power budget. Therefore, the operational procedure consisted of turning on the transmitter, sending some images, power cycling the transmitter and repeating. If the receiver is not synchronised to a satellite's signal, it sweeps the frequency of the local oscillator (brown) across the frequency range in search of a signal every 2 s while at the same time the gain (light blue) is also swept at a frequency that is ten times higher. Once a signal is found the local oscillator follows the signal and thus the graph shows the expected Doppler shift curve. The gain on the other hand tries to compensate the measured signal-to-interference ratio (SIR) to generate a consistent output power level. Additionally it can be seen, that the temperature of the S band transmitter onboard BEESAT-3 increases during its use, but does not reach any critical level within the duration of a pass.

Moreover, this was the last pass with a successful transmission of a full image. The last row of the diagram in Figure 5 shows the size of payload data per transmitted packet (orange, left axis) and the reached transmission speeds (darkgreen, right axis). The first image transmission can be seen between 12:06:17 UTC and 12:06:25 UTC, while the second one was interrupted by the desync at 12:06:43 UTC. During the second longer sync other data was transmitted and thus the graphs are looking different.

At 12:09:45 UTC the SIR sinks below 4 dB whereupon the receiver decides to desync and re-establish the contact, here that took only 1.64 s. This is displayed again on the right side of Figure 5 with a higher temporal resolution showing the sweeping behaviour of the local oscillator and receiver gain.

As the TU Berlin S band ground station has a comparably small opening angle of 3°, the increasing position inaccuracies discussed in Section 5 became a problem and the last synchronisation be-

tween satellite and ground station occurred at 2023-12-21. Hence it was later only possible to see transmissions of the HiSPiCO S band transmitter with ground stations of the SatNOGS network that feature a omnidirectional antenna. Thereby the latest transmission were observed on 2023-12-27 at 21:25:05, 21:26:25 and 21:27:51 in the three SatNOGS observations from stations in the Netherlands and Switzerland [21], within 48 h before re-entry. It is believed that these observations are showing only the unmodulated base band as it is transmitted after turning on the transmitter. The times correspond with the commands sent out to turn on the HiSPiCO, but before actual payload data is send.

Overall it could be shown that the HiSPiCO S band transmitter of BEESAT-3 was still functional after more than 10 years in orbit. Thereby, both the transmitted status data and the payload data was well received and decodable.

5 MITIGATING TLE POSITION INACCURACIES

All satellites are tracked by NORAD through regularly measurements. The determined orbital elements are then published as TLE 1-2 times a day per satellite. For normal satellite operation with an altitude between 400 km to 500 km, at least inside the BEESAT family, the TLEs are sufficient enough as their accuracy within one day is about 2.34 km [22]. During ADCS experiments the accuracy of a maneuver is mostly limited by the attitude control system (sensors precision and noise, control of actuators). To communicate with the BEESATs the ground stations use UHF cross yagi antennas with opening angles between $10° - 20°$ and an antenna gain of 17.95 dBi – 22 dBi. An effect on the communication link can be observed when the satellites actual position differs to much from the predicted position and the satellite is outside of the main lobe of the ground station antenna. As described in Table 1 the BEESATs transmit on a fixed frequency and therefore the Doppler frequency correction has to be applied by the ground station. An inaccuracy in the position prediction causes an inaccuracy in relative velocity leading to the wrong Doppler frequency correction being applied to the signal. If the actual signal frequency shift is too far away from the calculated shift, the signal can no longer be decoded.

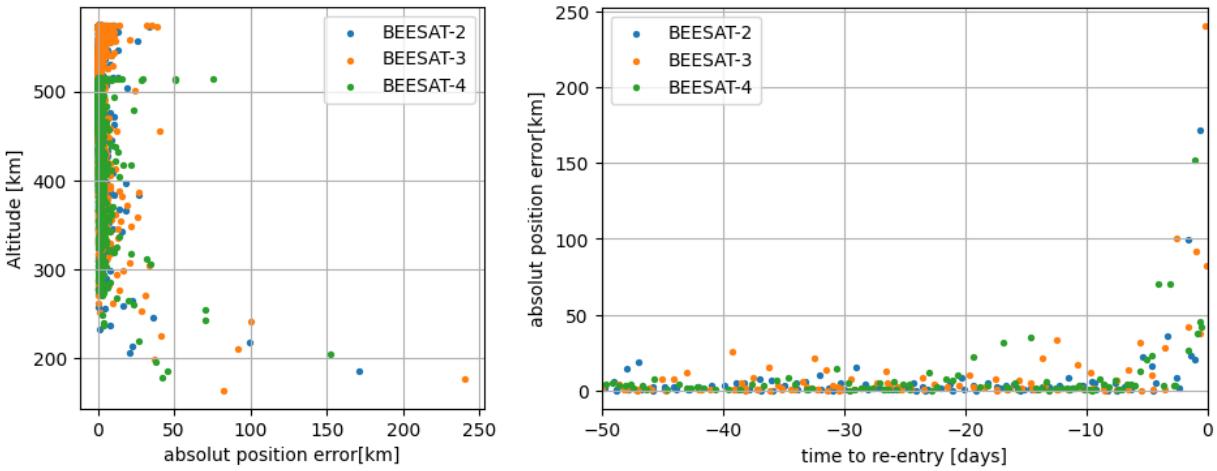

(a) In Respect to Altitude

(b) In Respect to Time to Re-entry

Figure 6: Position Error Between Old and New TLEs for the BEESATs

There are two situations where the satellite position calculated from TLEs can be problematic. Firstly in the LEOP the satellites position right after separation can only be estimated from calculations in-

corporating the launch vehicles position, orientation and release velocity. Within hours to days NORAD finds the new objects, but especially with recent mass launches of dozens small satellites it can take some time until a catalog ID can be assigned to a satellite with certainty. Secondly in situations were the satellites orbit changes rapidly TLEs and the underlying Simplified General Perturbations model 4 (SGP4) model can not predict the position accurately. These situations can be a result of propulsive maneuvers or rapidly increasing atmospheric drag as experienced in VLEO right before a re-entry. Figure 6a shows the position difference between the propagation with the previous TLE and the new TLE throughout the BEESATs missions. Increased inaccuracies are visible during the LEOP phase and when the atmospheric drag rapidly increases below approximately $250\,\mathrm{km}$.

5.1 Mitigation Strategies

To mitigate the problems that come with TLE position inaccuracies different strategies were applied during the three consecutive re-entries. As there were multiple weeks to months between them, the time was used to advance these strategies or adapt new ones. The remaining part of this section will describe the strategies and their challenges during the three re-entries.

5.1.1 Satellite Tracking Through Radio Observations

The satellite tracking toolkit for radio observations (STRF) software provides a package to analyse IQ data previously recorded with an SDR [23]. The first use case is to identify satellite signals by the Doppler shifted transmissions. Therefore using the *rfplot* software the Doppler curves of newly found spacecraft objects are plotted in the waterfall diagram generated from the IQ data recording. By comparing the satellite transmissions with the predicted curves an identification is possible, while additionally knowledge about the modulation type of the signal and thereby appearance in the diagram can help. A second use case is to detect a deviation of the signals from the predicted Doppler shift. After detecting a deviation in *rfplot* the satellite's transmissions can be exported to *rffit*, which is another software from the STRF package. There the measurements can be used to fit an existing TLE set to better align with the observations.

During the BEESAT-4 re-entry campaign, radio amateurs from the SatNOGS community recorded IQ data for the analysis with STRF and generated new TLEs from that. As this proved useful once the inaccuracy problems occurred, a new SDR ground station at TU Berlin was established to perform own STRF measurements. After the initial setup in December 2023 in preparation of the BEESAT-3 re-entry campaign a new challenge emerged: Normally the IQ data recordings are showing only the signals from the observed satellite as the ground station from the satellite operator is not nearby. However the BEESATs are operating in half-duplex mode sharing the same frequency for up- and downlink and all Berlin ground stations of TU Berlin are located on the same roof. So even when not pointing directly at each other the side lobes of the signals sent from the telecommand and telemetry ground station are coupling into the STRF ground station. As the signal strength of the transmission from the ground station is up to $60\,\mathrm{dB}$ stronger than those from the satellite and due to the internal structure of the SDR they raise the intensity of the complete spectrum. As a result the satellite transmissions necessary for the STRF analysis can not be seen and analysed as the later is done by highest power in the spectrum.

This challenge was solved by making two changes to the standard procedure:

- Firstly by changing the scaling of the power density in the waterfall diagram to a much smaller range, faint signals such as those from the satellite become visible. As a side effect not only

the part of the spectrum where the actual telecommand is transmitted, but the completely raised spectrum crosses the maximum displayable power density.

- Secondly in the process of converting the IQ data to spectral density with the *rffft* software a fast Fourier transform is conducted followed by binning on the time axis. With the standard time of 1.0 s for a bin, transmissions from the ground station (telecommands, acknowledgements) were often in the same bin as the satellites telemetry. By reducing the time to 0.1 s it was possible to separate the transmissions and thereby making the data analysis possible.

In Figure 7 the process of generating a new TLE set is visualized based on the two latest BEESAT-2 passes prior to re-entry. Firstly in Figure 7a the spots with the highest spectral density are found within the spacecrafts telemetry transmissions. After filtering out the spots found in SDR artifacts originating from ground station transmissions and noise, the spots are used in Figure 7b to fit the latest, but at this time more than 10 h (epoch) old, TLE against them. Finally Figure 7c shows the IQ data from the last BEESAT-2 pass with the predicted Doppler shift from both the latest published and the new generated TLE. It can be seen that the new STRF TLE fits the spacecraft transmissions much better than the old one.

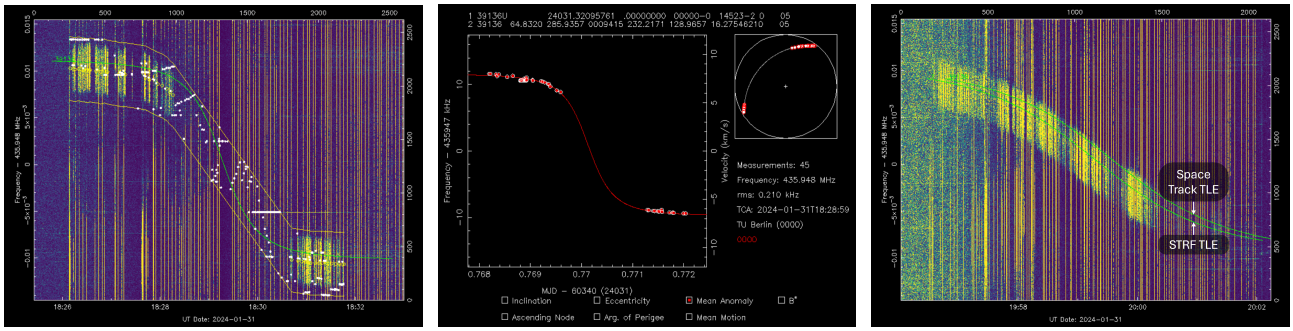

(a) *rfplot* of Second to Last Pass: Finding Spots of Highest Spectral Density (white) in Waterfall Plot.

(b) *rffit* of Second to Last Pass: Fitted the Old Space Track TLE to 45 Found Spots with a root mean square (RMS) of 210 Hz.

(c) *rfplot* of Last Pass: The Newly Generated TLE Fits the Satellites Transmissions Much Better than the Space Track TLE.

Figure 7: Process of Generating a New TLE and Using it in the Following Pass During the Two Last Passes of BEESAT-2 Prior to its Re-Entry, Passes Started on 2024-01-31 at 18:26:06 UTC and 19:56:28 UTC.

5.1.2 GNSS

A potentially better solution to mitigate position inaccuracies would be to determinate the position on-board the satellite using a Global Navigation Satellite System (GNSS) receiver as the accuracy is higher than the previously discussed methods. A disadvantage is the necessity that the satellite must still be able to communicate with a ground station properly to transmit the GNSS data. As none of the BEESATs discussed in this paper feature a (functional) GNSS receiver this could not be investigated in the scope of this publication. Newer TU Berlin satellites as the successor BEESAT-9 and the newer TUBSATs TU Berlin Infrared Nanosatellite (TUBIN) and NanoFF A & B have one or more GNSS receiver that could enhance the position determination.

6 ATTITUDE DETERMINATION and CONTROL in a VLEO ENVIRONMENT

Due to increasing interactions with the upper atmosphere and possibly less accurate environmental models at lower altitudes, the ADCS is monitored closely while in VLEO.

After the ongoing ADCS experiments were concluded, during the final days before the re-entry of BEESAT-4 an unusual rapid increase in angular rates could be observed. This can be seen in Figure 8a depicting the angular rates of BEESAT-4 in the spacecraft frame. The absolute rates shown in Figure 8 are calculated according to Equation (1).

$$\omega = \sqrt{\omega_x^2 + \omega_y^2 + \omega_z^2} \tag{1}$$

This results in the necessity for frequent damping of the angular rates with the magnetic coils. After damping, the angular rates resumed to increase rapidly. The same phenomenon could be observed during the re-entry of BEESAT-2. The angular rates of BEESAT-2 in the spacecraft frame can be seen in Figure 8b. As BEESAT-2 had less ADCS activity in the time leading up to re-entry, the spin up could be observed over a longer time frame.

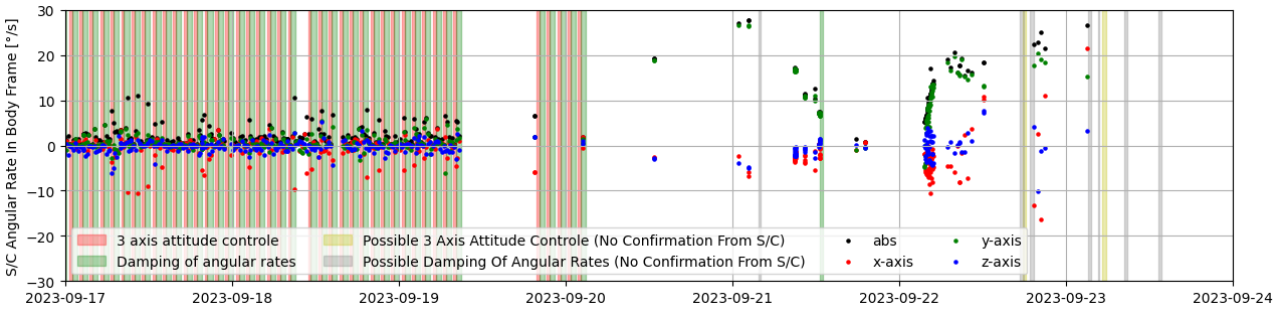

(a) Angular Rates of BEESAT-4 Prior to Re-Entry

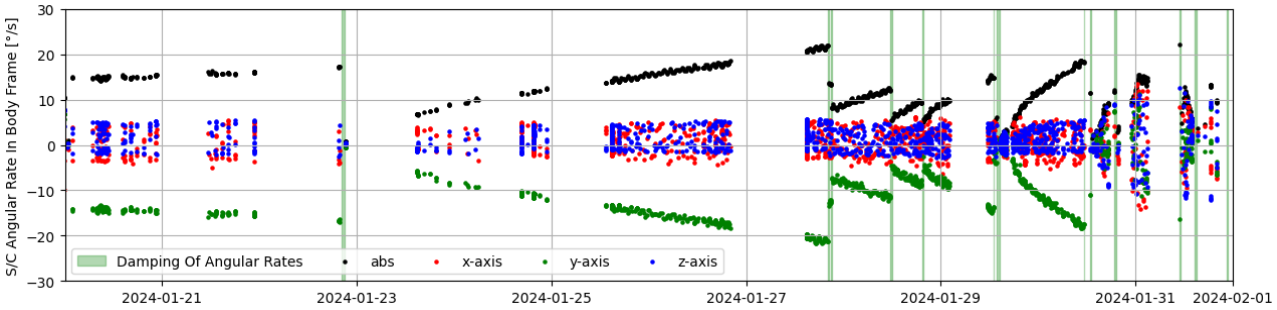

(b) Angular Rates of BEESAT-2 Prior to Re-Entry

Figure 8: Angular Rates of the BEESATs Prior to Re-Entry

Notably, during both re-entries, the angular rate was mostly concentrated on the y-axis. It is assumed that this is due to interactions of the deployed antennas with the upper atmosphere. Data from BEESAT-3 is not taken into account as its passive ADCS with a permanent magnet and a hysteresis plate differs from the other BEESATs.

For further analyses of the spin up, the absolute angular momentum of BEESAT-2 is calculated from the recorded angular rate $\vec{\omega}$ in the body-fixed reference frame. The absolute angular momentum L is calculated according to Equation (2) for every telemetry data point where the spacecraft is tumbling without active attitude control actuators.

$$L = \left|\vec{L}\right| = |I \cdot \vec{\omega}| \tag{2}$$

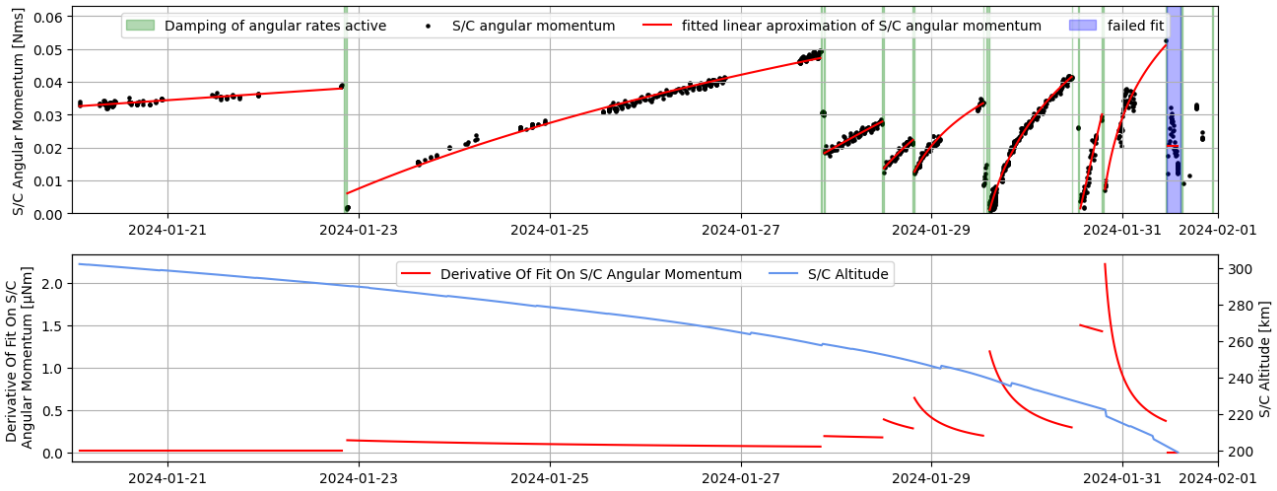

Figure 9: Fitting Gain of Angular Momentum over Time and Altitude

For this, an estimated inertia tensor I_{b2} of BEESAT-2 is provided by TU Berlin:

$$I_{b2} = \begin{bmatrix} 2495.41 & 0.0 & 0.0 \\ 0.0 & 2227.98 & 0.0 \\ 0.0 & 0.0 & 2548.43 \end{bmatrix} \text{kgmm}^2 \tag{3}$$

To better characterize the increase in angular momentum L, as a first step the logarithmic function defined in Equation (4) is fitted to each distinct tumbling phase with more than 20 data points. Further analysis regarding the underlying physical model is needed and will be done in the scope of the BEESAT-9 re-entry.

The resulting functions are shown in red in the upper half of Figure 9. The fit fails for the second to last tumbling phase highlighted in blue as there is an equally strong downward trend. The reason for this downward trend is still unknown and further investigation is needed to determine the underlying cause.

$$L(t) = A * ln^{t+B} + C \tag{4}$$

The change in angular momentum L is quantified as the derivative of the angular momentum $\dot{L}$:

$$\dot{L}(t) = \frac{A}{t+B} \tag{5}$$

The derivative of the fitted angular momentum is shown in the lower half of Figure 9. This figure also shows the current altitude of the spacecraft according to the TLEs on a secondary axis. The discontinuities in the spacecraft altitude correspond to TLE updates.

The lower half of Figure 9 shows an increase in angular momentum L over the complete dataset* with larger increases beginning 4 days before re-entry or around 250 km. This analysis is only done for BEESAT-2 as there is not enough data available from the spin up phases of BEESAT-4. As high angular rates can lead to communication issues [24] it is important to closely monitor the angular rates prior to reentry or in general within the VLEO environment.

The blind damping of BEESAT-2 and BEESAT-4 remained effective through out re-entry operations as the angular rates were reduced when in damping mode.

*with the exception of the second to last tumbling phase

7 CONCLUSION

This work shows the robustness of the BEESAT satellite bus. It is notable that such a CubeSat mainly consisting of COTS parts with the example of BEESAT-2 remained operational in orbit for over a decade. All other iterations with shorter overall orbit dwell times but further payload capabilities remained functional beyond their planned mission lifetime and until re-entry as well. It is also shown that crucial subsystems like the ADCS and EPS or payloads like the BEESAT-3 S band transmitter do not show critical degradation. Operations until their natural EOL gave the opportunity to gather insights into systems' behaviour in the VLEO environment. It is confirmed that orbit determination and tracking is challenging with CubeSats during the last five days of operations below an orbit height of 250 km. For future missions targeting VLEO or aiming to operate as long as possible it is recommended to rely on an independent positioning like a GNSS receiver or a solution like STRF. Furthermore, a spin-up of angular rates is observed in this region. The BEESATs were capable of damping these rates via magnetorquers. For future missions it may be recommended to model the aerodynamic behaviour in advance and to avoid sources for additional unbalanced drag like wide antennas or other extensions. During EOL operations angular rates should be observed and damped if necessary. These measures will be taken into account during the final days of BEESAT-9 whose re-entry is imminent in 2024. Its bus is identical to the CubeSats discussed in this paper and it carries a GNSS receiver payload. With this setup it will give another opportunity to apply the lessons learned documented in this paper which will be the scope of future work.

Acknowledgements

The authors would like to thank the DLR for funding the BEESAT projects and Universidad Nacional de San Martín for hosting the San Martín ground station. They thank the whole amateur radio community for supporting the re-entry campaigns with conducting satellite observations and providing IQ data-recordings as well as support for various software used. Special mentions have to be given to Alfredos-Panagiotis Damkalis (SatNOGS administrator), Cees Bassa (STRF) and Kevin Croissant, James Cutler (University of Michigan), Alexander Spaniol (Fachhochschule Wiener Neustadt), Jan Van Gils, Daniel Ekman, Vladimir E. Cherny (Belarusian State University) and Oleg Soroka (Kyiv Polytechnic Institute).

References

[1] "NanoFF." (2023), [Online]. Available: `https://www.tu.berlin/raumfahrttechnik/forschung/aktuelle-projekte/nanoff` (visited on 04/09/2024) (cit. on p. 1).

[2] S. Trowitzsch, F. Baumann, and K. Brieß, "BEESAT-2 – A Picosatellite Demonstrating Three-Axis Attitude Control with Reaction Wheels," in *62. Deutscher Luft- und Raumfahrtkongress*, 2013 (cit. on p. 2).

[3] M. F. Barschke, P. Werner, and S. Kapitola, "BEESAT-3 commissioning – better late than never," in *Proceedings of the 69th International Astronautical Congress*, 2018 (cit. on pp. 2, 8).

[4] M. Wermuth and G. Gaias, "Operational Concept of a Picosatellite Release from a LEO Satellite," 2015 (cit. on p. 2).

[5] S. Kapitola, S. Weiß, and K. Brieß, "Flight experience and operations with the cubesat beesat-4," in *11th IAA Symposium on Small Satellites for Earth Observation*, 2017 (cit. on p. 2).

[6] T. Erdmann, S. Kapitola, and C. Avsar, "Implementation of a satellite operations student project in the multi-mission context at tu berlin," in *70th International Astronautical Congress*, 2019 (cit. on p. 2).

[7] T. Erdmann and M. Krachten, "Lessons-learned from teaching satellite operations in a novel hands-on student project utilizing in-orbit spacecraft during the covid-19 pandemic," in *4th Symposium on Space Educational Activities*, Universitat Politècnica de Catalunya, 2022 (cit. on p. 2).

[8] L. Berthoud, R. Hills, A. Bacon, *et al.*, "Are Very Low Earth Orbit (VLEO) satellites a solution for tomorrow's telecommunication needs?" *CEAS Space Journal*, vol. 14, no. 4, pp. 609–623, 2022 (cit. on p. 3).

[9] V. Ray, T. E. Berger, Z. C. Waldron, *et al.*, "The impact of space weather on very low Earth orbit (VLEO) satellites," in *Advanced Maui Optical and Space Surveillance Technologies (AMOS) Conference*, 2022 (cit. on p. 3).

[10] C. Pardini and L. Anselmo, "Re-entry predictions for uncontrolled satellites: Results and challenges," in *6th IAASS Conference-Safety is Not an Option*, Citeseer, 2013 (cit. on p. 3).

[11] L. Anselmo and C. Pardini, "Computational methods for reentry trajectories and risk assessment," *Advances in Space Research*, vol. 35, no. 7, pp. 1343–1352, 2005 (cit. on p. 3).

[12] T. Kelso, *Celestrak*. [Online]. Available: `https://celestrak.org` (cit. on p. 3).

[13] S. P. Hughes, "General Mission Analysis Tool (GMAT)," NASA Goddard Space Flight Center Greenbelt, MD, United States, Tech. Rep., 2007. [Online]. Available: `https://ntrs.nasa.gov/citations/20080045879` (cit. on p. 3).

[14] J. Kennewell, "Satellite orbital decay calculations," *Australian Space Weather Agency*, vol. 111, 1999 (cit. on p. 3).

[15] A. L. Cauchy, *Mémoire sur la rectification des courbes et la quadrature des surfaces courbes par M. Augustin Cauchy*. Lith. de C. Mantoux, 1832 (cit. on p. 4).

[16] N. Gress, T. L. Kirsch, T. Erdmann, B. Akyil, and et al, "Utilizing small satellites with earth observation capabilities for satellite operations education," in *13th IAA Symposium on Small Satellites for Earth Observation*, 2021 (cit. on p. 7).

[17] K. Croissant, D. White, X. C. Álvarez, *et al.*, "An Updated Overview of the Satellite Networked Open Ground Stations (SatNOGS) Project," 2022 (cit. on p. 7).

[18] ITU Radio Regulations, "I - Amateur Service, 25.2A § 2," "Transmissions between amateur stations of different countries shall not be encoded for the purpose of obscuring their meaning, except for control signals exchanged between earth command stations and space stations in the amateur-satellite service." (cit. on p. 7).

[19] *GNU Radio*. [Online]. Available: `https://www.gnuradio.org/` (cit. on p. 8).

[20] SatNOGS, *SatNOGS observation 8966521*, [Online]. Available: `https://network.satnogs.org/observations/8966521/` (cit. on p. 8).

[21] SatNOGS, *BEESAT-3 S band observations*, [Online]. Available: `https://network.satnogs.org/observations/8771789/`, `https://network.satnogs.org/observations/8771797/`, and `https://network.satnogs.org/observations/8775799/` (cit. on p. 10).

[22] R. Wang, J. Liu, and Q. Zhang, "Propagation errors analysis of tle data," *Advances in Space Research*, vol. 43, no. 7, pp. 1065–1069, 2009 (cit. on p. 10).

[23] C. Bassa, *Satellite tracking toolkit for radio observations*. [Online]. Available: `https://github.com/cbassa/strf` (cit. on p. 11).

[24] L. Volk, R. Borrek, N. Zischka, *et al.*, "New results and lessons learned from the move-ii and move-iib cubesats," 2022 (cit. on p. 14).

Acronyms

ADCS attitude determination and control system. 4, 5, 10, 13, 15

API application programming interface. 7

BEESAT Berlin Experimental and Educational Satellite. 1–15

BIROS Bi-spectral InfraRed Optical System. 2

COM Communication System. 8

COTS Commercial-off-the-shelf. 5, 15

DLR Deutsches Zentrum für Luft- und Raumfahrt. 2

EOL End Of Life. 3, 5, 7, 8, 15

EPS Electrical Power System. 4, 15

FIFO First In First Out. 8

GNSS Global Navigation Satellite System. 12, 15

GPS Global Positioning System. 2

HiSPiCO Hochintegrierter S-Bandsender für Pico- und Nanosatelliten. 8–10

IQ in-phase and quadrature components of a radio signal. 8, 11, 12, 15

ITU International Telecommunication Union. 7

LEO Low Earth Orbit. 2

LEOP Launch and Early Orbit Phase. 6, 10, 11

MCU microcontroller unit. 5

NanoFF Nanosatellites in Formation Flight. 1, 12

NORAD North American Aerospace Defense Command. 3, 10, 11

PCU Power Control Unit. 5

PDH Payload Data Handling. 5

RF radio frequency. 8

RMS root mean square. 12

SatNOGS Satellite Networked Open Ground Station. 7, 8, 10, 11, 15

SatOps project lab Satellite Operations. 7

SDR software-defined radio. 7, 11, 12

SGP4 Simplified General Perturbations model 4. 11

SIR signal-to-interference ratio. 9

STRF satellite tracking toolkit for radio observations. 11, 12, 15

StudOps TU Berlin Student Satellite Operation Team. 2, 7

TLE two-line element. 3, 7, 8, 10–12, 14

TRX Transceiver. 5

TU Berlin Technische Universität Berlin. 1, 7–9, 11, 12, 14

TUBIN TU Berlin Infrared Nanosatellite. 12

TUBSAT TU Berlin Satellite. 1, 12

UHF ultra high frequency. 8

VLEO Very Low Earth Orbit. 3, 8, 11, 13–15